



# Structural characteristics and high-temperature tribological behaviors of laser clad NiCoCrAlY–B<sub>4</sub>C composite coatings on Ti6Al4V alloy

Wen-chang WANG<sup>1</sup>, Jia-xing LI<sup>2</sup>, Yuan GE<sup>3</sup>, De-jun KONG<sup>2</sup>

1. School of Petrochemical Engineering, Changzhou University, Changzhou 213164, China;
2. School of Mechanical Engineering, Changzhou University, Changzhou 213164, China;
3. Meltron Metal Surface Technology (Changzhou) Co., Ltd., Changzhou 213164, China

Received 10 September 2020; accepted 10 May 2021

**Abstract:** In order to improve the hardness and tribological performance of Ti6Al4V alloy, NiCoCrAlY–B<sub>4</sub>C composite coatings with B<sub>4</sub>C of 5%, 10% and 15% (mass fraction) were fabricated on its surface by laser cladding (LC). The morphologies, chemical compositions and phases of obtained coatings were analyzed using scanning electronic microscope (SEM), energy dispersive spectrometer (EDS), and X-ray diffraction (XRD), respectively. The effects of B<sub>4</sub>C mass fraction on the coefficient of friction (COF) and wear rate of NiCoCrAlY–B<sub>4</sub>C coatings were investigated using a ball-on-disc wear tester. The results show that the NiCoCrAlY–B<sub>4</sub>C coatings with different B<sub>4</sub>C mass fractions are mainly composed of NiTi, NiTi<sub>2</sub>,  $\alpha$ -Ti, CoO, AlB<sub>2</sub>, TiC, TiB and TiB<sub>2</sub> phases. The COFs and wear rates of NiCoCrAlY–B<sub>4</sub>C coatings decrease with the increase of B<sub>4</sub>C content, which are contributed to the improvement of coating hardness by the B<sub>4</sub>C addition. The wear mechanisms of NiCoCrAlY–B<sub>4</sub>C coatings are changed from adhesive wear and oxidation wear to fatigue wear with the increase of B<sub>4</sub>C content.

**Key words:** Ti6Al4V alloy; laser cladding; NiCoCrAlY coating; B<sub>4</sub>C; tribological behavior; wear

## 1 Introduction

Ti6Al4V alloy is widely used in aerospace, medical and weapon fields due to its low density, high strength and corrosion resistance [1,2], which accounts for 50% of the total consumption amount of Ti alloys. However, its poor wear resistance limits the application fields due to its low hardness [3,4]. Scholars have tried to solve this problem, and found that coating technology is the main method of improving the hardness of Ti6Al4V alloy. As excellent thermal barrier coatings, MCrAlY (M=Ni, Co or combination of these) coatings are applied to protecting the substrate from oxidation at high temperature. PEREIRA et al [5] prepared the NiCoCrAlY and CoNiCrAlY coatings on AISI 304 steel by laser cladding (LC), showing

that the coefficient of friction (COF) of Ni-based coating was lower than that of Co-based coating at 500 °C. Meanwhile, PEREIRA et al [6] also revealed that the NiCoCrAlY coating prevented further the oxidation of substrate by forming a thermally-grown oxide (TGO) film at 1100 °C. The research results also show that the NiCoCrAlY coating increases the wear resistance at high temperature for all materials tested [5], which is a promising coating in the tribological fields.

At present, LC is an effective method of directed energy deposition (DED) for the NiCoCrAlY coating, in which argon gas is used to prevent the formation of oxide film in the coating fabrication process [7]. As a covalent bond compound, B<sub>4</sub>C has excellent physical properties, such as high melting point, low density and hardness is second only to diamond and CBN [8],

which is widely used in the light ceramic armor, wear resistance parts and coating materials [9].

In the past, a lot of researches have been done on the  $B_4C$  reinforced Ni-based coatings. ZHAO et al [10] prepared the Ni204 coatings with the different mass fractions of TiC, TiN and  $B_4C$  on 45 steel by LC, and found that their COFs decreased compared with the Ni204 coating. PUSHPANATHAN et al [11] developed the Ni- $B_4C$ -TiC coating on AZ80 alloy, and revealed that the grain refinement of nickel and orientation of nano-particles improved the coating properties. And MENG et al [12] fabricated the NiCrBSi-5% $B_4C$  coating on Ti-6Al-4V substrate by LC, and indicated that  $B_4C$  was reacted with the Ti of substrate, which in-situ synthesized the  $TiB_2$  and TiC reinforcements in the coating. The above analyses show that the  $B_4C$  reinforced phase improved the hardness and friction-wear performances of MCrAlY coatings. However, few reports on the in-situ synthesis and tribological performance of NiCoCrAlY- $B_4C$  coating on Ti6Al4V alloy have been reported.

In this study, NiCoCrAlY coatings with the different  $B_4C$  mass fractions were fabricated on Ti6Al4V alloy using a LC. The aim was to in-situ synthesize the TiC, TiB and other ceramic phases by  $B_4C$  and Ti of Ti6Al4V alloy, and the effects of  $B_4C$  mass fraction on the microstructure and high temperature wear resistance of obtained coatings were studied, which provided the experimental data for the tribological fields of NiCoCrAlY- $B_4C$  coatings at high temperature.

## 2 Experimental

### 2.1 Sample preparation

The substrate was Ti6Al4V alloy with the chemical composition (wt.%): Fe  $\leq 0.30$ , C  $\leq 0.10$ , N  $\leq 0.05$ , H  $\leq 0.015$ , O  $\leq 0.20$ , Al 5.5–6.8, V 3.5–4.5, and Ti balance. NiCoCrAlY powders (Chengdu Huayin Powder Technology Limited Company, China) with the  $B_4C$  mass fractions of 5%, 10% and 15% (Hebei Yili Metallurgical Materials Limited Company, China) were milled using a planetary ball miller for 2 h. The LC test was conducted on a ZKSX-2008 type fiber-coupled LC system (Jiangsu Zhongke Sixiang Laser Technology Limited Company, China), and the powder feeding was conducted using a LAMCN-C type nozzle with the

coaxial ring. Technique parameters were: laser wavelength of 1064 nm, beam distribution of circular Gaussian, spot diameter of 4 mm, laser power of 1400 W, scanning speed of 4 mm/s, stand-off distance of 50 mm, and overlap rate of 50%.

### 2.2 Characterization methods

The surface morphologies, cross-section microstructure and phases of obtained coatings were analyzed using JSM-6360LA type scanning electron microscopy (SEM), VHX-700F type ultra-depth microscope (UDM), and D/Max-2500/PC type X-ray diffraction (XRD), respectively. The hardness was measured using a micro Vickers hardness tester, where the hardness was characterized with the average value in the three testes.

The friction and wear test was performed on a HT-1000 type high temperature wear tester with the ball-disk contact method. Test parameters were: friction pair of  $Si_3N_4$  ball, temperature of 600 °C, rotation speed of 500 r/min, normal load of 4.5 N, and time of 30 min. The profiles, morphologies, chemical elements of worn tracks on the NiCoCrAlY- $B_4C$  coatings were analyzed using UDM, SEM, and EDS, respectively.

## 3 Results and discussion

### 3.1 Morphologies and XRD analysis of powders

The morphologies of NiCoCrAlY powders with the  $B_4C$  mass fractions of 5%, 10% and 15% are shown in Figs. 1(a–c), respectively. The three kinds of mixed powders had no obvious differences, which were composed of NiCoCrAlY and  $B_4C$  powders. Figure 1(d) shows the XRD patterns of NiCoCrAlY- $B_4C$  powders. The mixed powders were mainly composed of Ni, Co, Cr and Al phases, and the  $B_4C$  peak was found at  $2\theta$  values of 23.50°, 34.96° and 37.82°; while the Y peak was not found due to its low content.

### 3.2 Characterization and analysis of coatings

#### 3.2.1 Morphologies and XRD analysis of coating

Figure 2(a) shows the surface morphology and XRD patterns of NiCoCrAlY coating. The coating was mainly composed of  $\alpha$ -Ti, NiTi,  $NiTi_2$  and CoO phases. The gray dendrite on the coating surface originated from the precipitation of  $\alpha$ -Ti and  $NiTi_2$  phases in the LC process. In this case, Ni

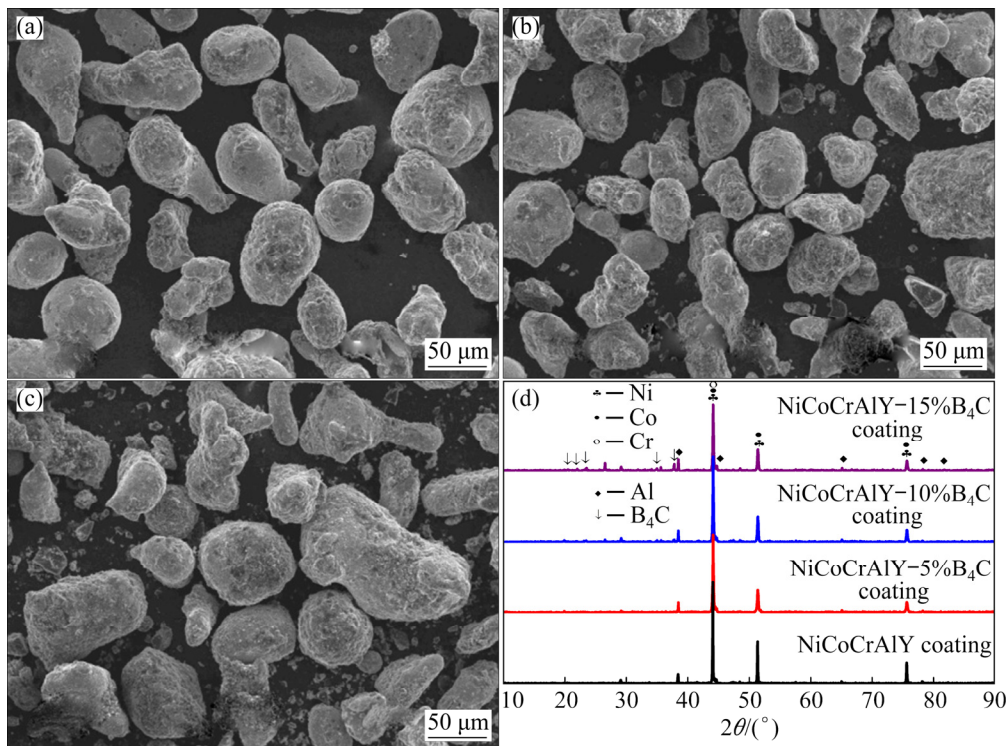


**Fig. 1** Morphologies of NiCoCrAlY powders with B<sub>4</sub>C mass fractions of 5% (a), 10% (b) and 15% (c), and XRD patterns of mixed powders (d)

was reacted with Ti of substrate as follows:



The NiTi and NiTi<sub>2</sub> in Eqs. (1) and (2) with the high contents were the basic phases of NiCoCrAlY coating, when the temperature exceeded the transformation temperature of  $\beta$ -Ti, the Ti went through the liquid phase (L) and transformation layers of  $\beta$ -Ti and  $\alpha$ -Ti+ $\beta$ -Ti, and the inhomogeneous distribution of elements easily produced the stress concentrations and cracks. Figure 2(b) shows the surface morphology and XRD patterns of NiCoCrAlY coating with the B<sub>4</sub>C mass fraction of 5%. The TiC, TiB, TiB<sub>2</sub> and AlB<sub>2</sub> phases were detected on the coating, and the B reduced the martensitic transformation temperature, which promoted the transformation from  $\beta$ -Ti to  $\alpha$ -Ti [13]. The B<sub>4</sub>C mainly was reacted with the Ti of substrate as follows [14]:



The dendrite structure was observed on the coating surface, which was because B<sub>4</sub>C was combined with the Ti of substrate. However, the

excess Ti precipitated and formed  $\alpha$ -Ti and NiTi<sub>2</sub> phases due to the low B<sub>4</sub>C content, which resulted in the dendritic segregation. There were a few pores, irregular black flakes and spherical particles on the coating surface, which were mainly composed of Ti and C with the NaCl type face centered cubic (FCC) structure. Figure 2(c) shows the surface morphology and XRD pattern of NiCoCrAlY coating with the B<sub>4</sub>C mass fraction of 10%. The coating porosity increased than the former coatings, and there was no new phase in XRD analysis result. Ti precipitated on the Ti-rich zones and was transformed into TiB and TiC phases with the increase of B<sub>4</sub>C mass fraction, and the dendrite crystal disappeared on the coating surface. Figure 2(d) shows the surface morphology and XRD patterns of NiCoCrAlY coating with the B<sub>4</sub>C mass fraction of 15%. There were many pores on the coating surface, and the dendrites disappeared, which was because the increase of B<sub>4</sub>C mass fraction neutralized Ti in the molten pool. Meanwhile, the amount of precipitated Ti was reduced, which prevented the dendrite segregation caused by the excessive dendrite precipitation. As a result, the in-situ synthesized ceramic phase refined the grain sizes and inhibited the crack growth [15].

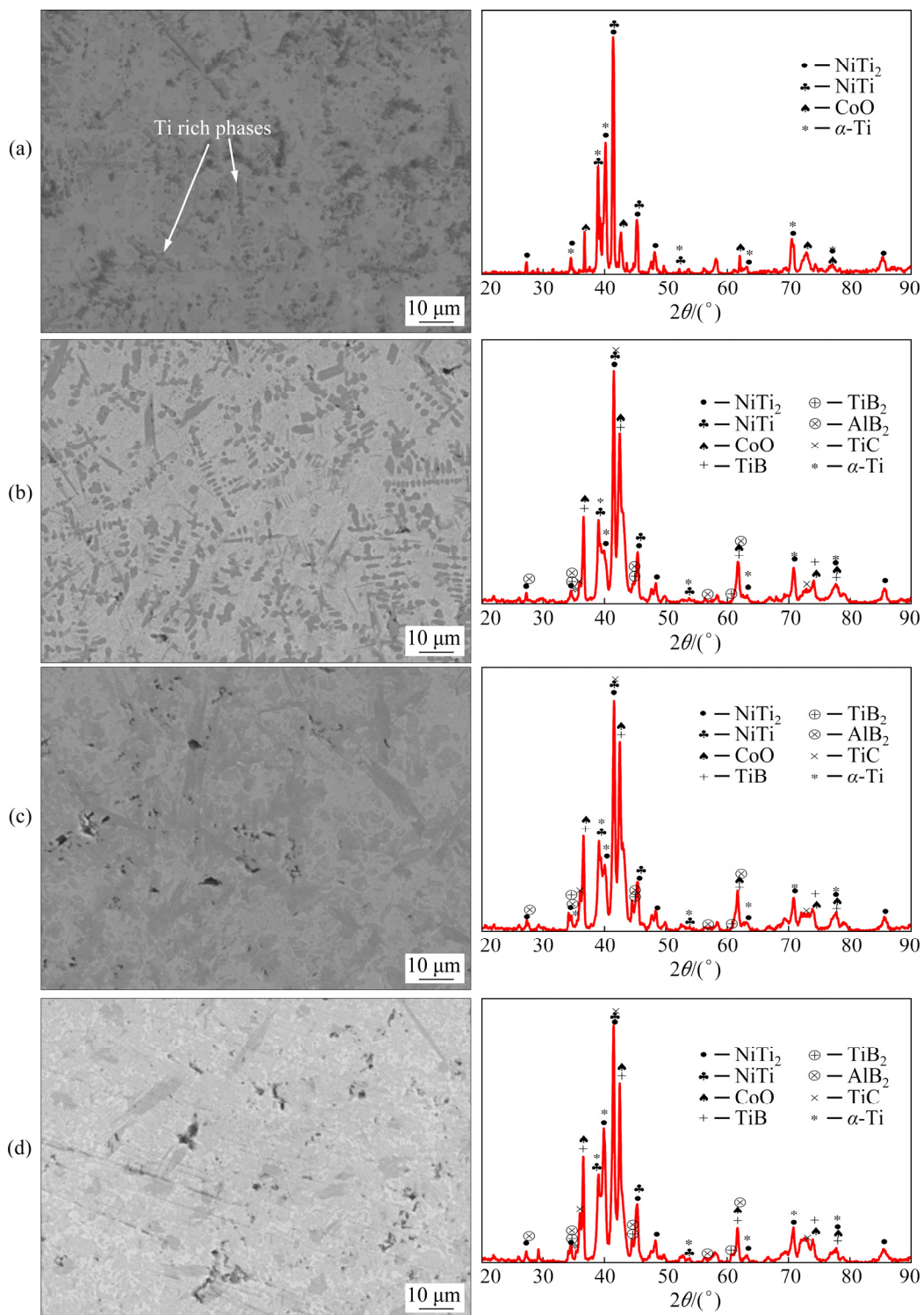


**Fig. 2** Morphologies and XRD patterns of NiCoCrAlY coating surfaces with B<sub>4</sub>C mass fractions of 0 (a), 5% (b), 10% (c) and 15% (d)

Figure 3(a) shows the morphology of the NiCoCrAlY coating cross-section. The bonding interface was serrated, which was because the heat conduction speed of the Ni-rich zone was faster than that of the Ti-rich zone. Figures 3(b–d) show the morphologies of the NiCoCrAlY–B<sub>4</sub>C coating

cross-sections. The number of pores decreased with the increase of B<sub>4</sub>C mass fraction, and there were no obvious boundaries between the coatings and the substrates, which indicated that the bonding mode at the coating interface was metallurgical bonding.

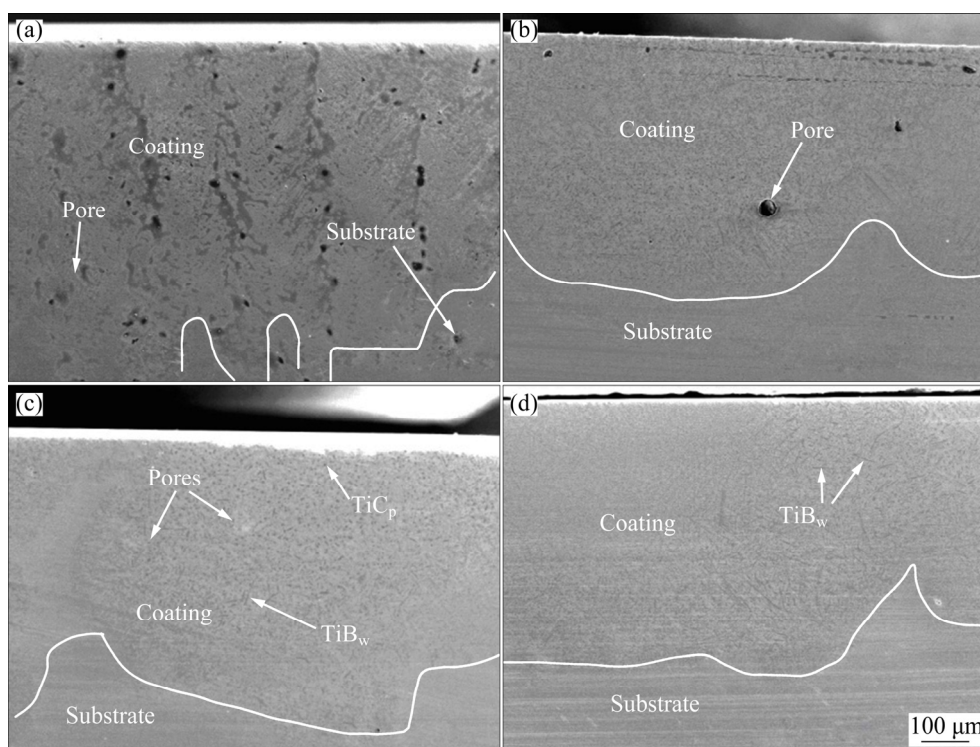


**Fig. 3** Morphologies of NiCoCrAlY coating cross-sections with B<sub>4</sub>C mass fractions of 0 (a), 5% (b), 10% (c) and 15% (d)

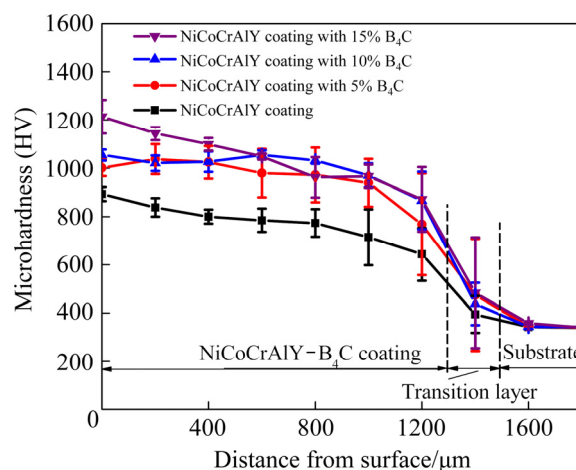
### 3.2.2 Hardness analysis

Figure 4 shows the hardness distributions of NiCoCrAlY–B<sub>4</sub>C coating cross-sections. The average hardness of NiCoCrAlY coating cross-sections with the B<sub>4</sub>C mass fractions of 5%, 10% and 15% were HV 1002, HV 1054, and HV 1213, respectively, higher than HV 893 of NiCoCrAlY coating. The increase of hardness was contributed to the TiC and TiB hard phases [16,17], meaning that the coating had the high micro cutting resistance and wear resistance [18]. There was an obvious hardness transition region between the coating and the substrate, which was because the contents of B and C on the coating bottoms were lower than those of TiC and TiB phases. Therefore, the hardness decreased rapidly on the transition zone. At the same time, the TiC and TiB phases increased the nucleation rate and refined the microstructure of NiCoCrAlY–B<sub>4</sub>C coatings, which further improved their hardness and wear resistance [19].

## 3.3 Friction and wear performances

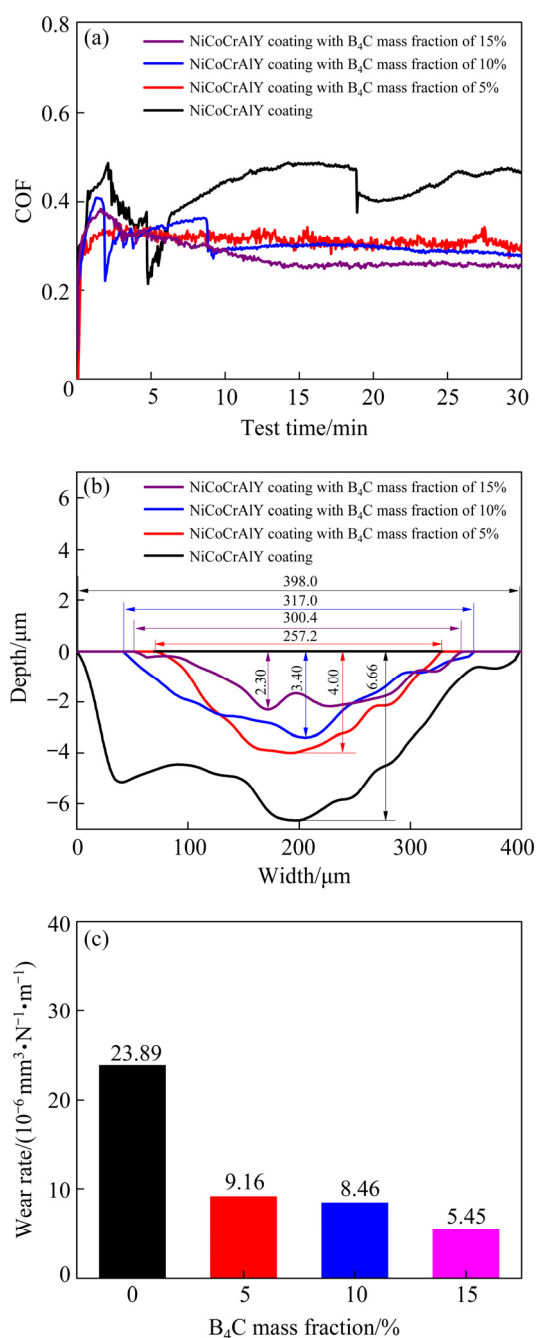
### 3.3.1 COFs and wear rates

Figure 5(a) shows the COFs of NiCoCrAlY–B<sub>4</sub>C coatings vs test time. The COFs fluctuated



**Fig. 4** Hardness distributions of NiCoCrAlY–B<sub>4</sub>C coating cross-sections

greatly in the running period, which were caused by the removal and redistribution of hard phases on the contact surface. The average COFs of NiCoCrAlY coatings with the B<sub>4</sub>C mass fractions of 5%, 10% and 15% in the normal period of 10–30 min were 0.31, 0.29, and 0.26, respectively, lower than 0.45 of NiCoCrAlY coating. The hard phases of NiCoCrAlY–B<sub>4</sub>C coatings prevented the formation of fine debris in the friction process, which played a role of friction reduction [20].



**Fig. 5** Curves of COF vs test time (a), profiles of worn tracks (b) and wear rates (c) on NiCoCrAlY–B<sub>4</sub>C coatings

Meanwhile, the graphite in the reaction processes of TiC and B<sub>4</sub>C acted as a lubricant to further reduce the COFs of NiCoCrAlY–B<sub>4</sub>C coatings. The standard deviation of NiCoCrAlY coatings with the B<sub>4</sub>C mass fractions of 5%, 10% and 15% were 0.0108, 0.0073, and 0.0072, respectively, lower than 0.0272 of NiCoCrAlY coating. The NiCoCrAlY–B<sub>4</sub>C coatings presented the smaller deviation, which was because B<sub>4</sub>C

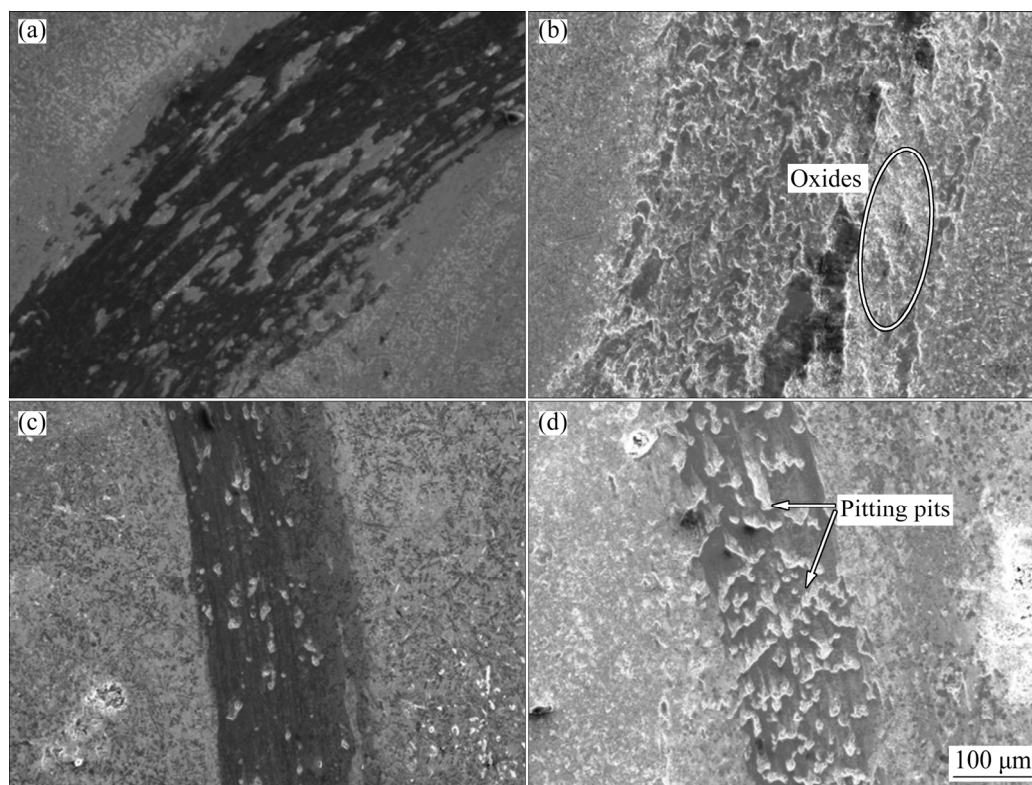
reduced the contents of  $\alpha$ -Ti and other oxides on the coating surface, which slowed down the COF fluctuations.

Figure 5(b) shows the profiles of worn tracks on the NiCoCrAlY–B<sub>4</sub>C coatings. The depths of worn tracks on the NiCoCrAlY coatings with the B<sub>4</sub>C mass fractions of 5%, 10% and 15% were 4.00, 3.40, and 2.30  $\mu\text{m}$ , respectively, which decreased with the increase of B<sub>4</sub>C mass fraction. The depths of worn tracks on the NiCoCrAlY–B<sub>4</sub>C coatings were smaller than 6.66  $\mu\text{m}$  of worn tracks on the NiCoCrAlY coating, which was because the TiC, TiB, TiB<sub>2</sub> and other hard phases hindered the wear of NiCoCrAlY–B<sub>4</sub>C coating [21]. Meanwhile, the graphite was acted as solid lubricant to reduce the COFs of NiCoCrAlY–B<sub>4</sub>C coating to a certain extent.

Figure 5(c) shows the wear rates of NiCoCrAlY–B<sub>4</sub>C coatings. The wear rates of NiCoCrAlY coatings with the B<sub>4</sub>C mass fractions of 5%, 10% and 15% were  $9.16 \times 10^{-6}$ ,  $8.46 \times 10^{-6}$ , and  $5.45 \times 10^{-6} \text{ mm}^3/(\text{N} \cdot \text{m})$ , respectively, which decreased by 61.63%, 64.58%, and 77.17% than  $23.89 \times 10^{-6} \text{ mm}^3/(\text{N} \cdot \text{m})$  of NiCoCrAlY coating, respectively. The hard phases of TiB and TiC were distributed on the coating surface [19], which played a role of friction reduction and wear resistance [22].

### 3.3.2 Worn morphologies and XRD analysis

Figure 6(a) shows the morphology of worn track on the NiCoCrAlY coating. There were obvious wear marks on the worn track, which was a typical adhesive wear feature. The coating oxides were produced on the worn track and pulled off by the tribo-pair, indicating that the oxidation wear occurred on the worn track. Figure 6(b) shows the morphology of worn track on the NiCoCrAlY coating with the B<sub>4</sub>C mass fraction of 5%. There was obvious plastic deformation on the worn track, and the adhesive wear was found on the worn track. The Ti of substrate was not reacted with the B<sub>4</sub>C due to the low content of B<sub>4</sub>C, which was oxidized to TiO<sub>2</sub> and fell off in the friction process. Figure 6(c) shows the morphology of worn track on the NiCoCrAlY coating with the B<sub>4</sub>C mass fraction of 10%. The smear marks disappeared on the worn track, which was because the amount of ceramic phases increased, and the sliding friction force was not enough to destroy them on the worn track,



**Fig. 6** Morphologies of worn tracks on NiCoCrAlY coatings with  $B_4C$  mass fractions of 0 (a), 5% (b), 10% (c) and 15% (d)

which reduced the degree of adhesive wear. However, there were some fatigue pits on the worn track due to the action of normal load, which fell off to form the fatigue pits on the worn track [23]. Figure 6(d) shows the morphology of worn track on the NiCoCrAlY coating with the  $B_4C$  mass fraction of 15%. The fatigue pits were the most serious among the four kinds of coatings. Meanwhile, the width of worn track became narrow, indicating that the wear resistance was improved to a certain extent, which was related to the enhancement of coating hardness. In this case, the thermal conductivities of TiC and TiB were much higher than those of Ti and  $TiO_2$ , which was the main factor of wear resistance for the NiCoCrAlY- $B_4C$  coatings [24].

Figure 7 shows the XRD patterns of NiCoCrAlY- $B_4C$  coatings. The new phases rutile- $TiO_2$  and  $(Ni, Co)_2Ti_4O$  were produced on the worn tracks, in which  $Ni_2Ti_4O$  was caused by the dissolution of O in  $NiTi_2$  [25], and  $Co_2Ti_4O$  was generated by the Co atom replacing the Ni atom in  $Ni_2Ti_4O$ . A small amount of  $\alpha$ -Ti on the worn track was oxidized to anatase- $TiO_2$ , which was irreversibly transformed into the rutile- $TiO_2$  [26], corresponding to the rutile peaks at  $2\theta$  values of  $27.45^\circ$ ,  $36.09^\circ$ ,  $39.19^\circ$  and  $41.23^\circ$ .

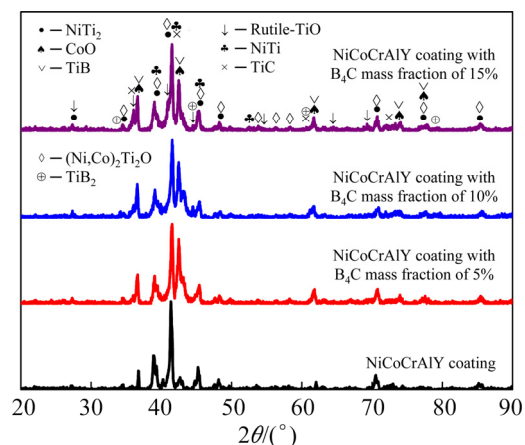


**Fig. 7** XRD patterns of worn tracks on NiCoCrAlY- $B_4C$  coatings

### 3.3.3 Line scan analysis of worn tracks

Figure 8(a) shows the line scanned position of worn track on the NiCoCrAlY coating, where C was the impurity products adsorbed on the coating surface in the air. The Ni content on the worn track decreased slightly than the unworn coating, which was because the  $NiTi_2$  was oxidized; while the Co, Cr, Al and Y contents on the worn track were no obvious change than the unworn coating, as shown in Fig. 8(b). The Ti content on the worn track decreased than the unworn coating due its oxidation;

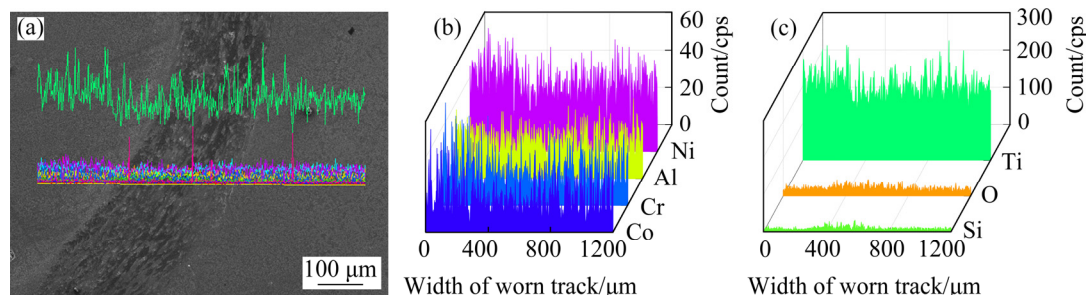
while the O content on worn track increased than the unworn coating due to the oxidation wear. And the Si content on the worn track increased than the unworn coating, which originated from the adhesion of tribo-pair, as shown in Fig. 8(c).

Figure 9(a) shows the line scanned position of worn track on the NiCoCrAlY coating with the B<sub>4</sub>C mass fraction of 5%. The Ni, Co and Cr contents did not change significantly; while the Al content on the worn track decreased than the unworn coating, which was worn away from the worn track, as shown in Fig. 9(b). The Ti content on the worn track increased than the unworn coating due to its oxidation, while the O content was the opposite. The Si content on the worn track increased slightly than the unworn coating, indicating that the wear mechanism was adhesive wear, as shown in

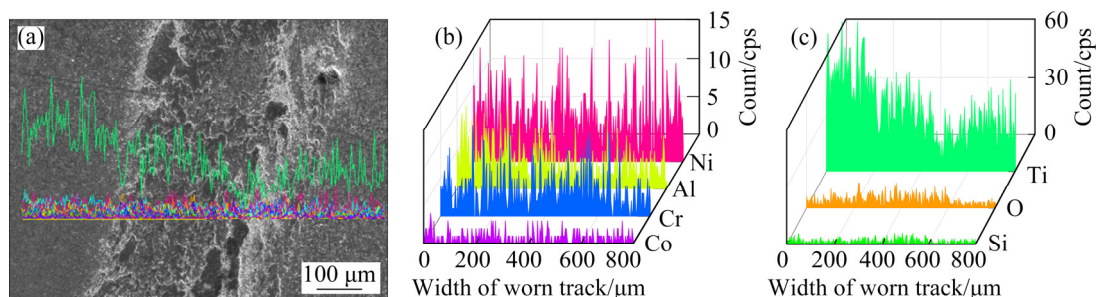
Fig. 9(c).

Figure 10(a) shows the line scanned position of worn track on the NiCoCrAlY coating with the B<sub>4</sub>C mass fraction of 10%. The Ni, Co and Al contents on the left side of worn track were high due to the uneven distribution of elements, as shown in Fig. 10(b). The Ti and O contents on the worn track decreased compared with those of the unworn coating, which was because the oxides were worn away from the worn track. And the Si content on the worn track increased compared with those of the unworn coating, indicating that the wear mechanism was adhesive wear, as shown in Fig. 10(c).

Figure 11(a) shows the line scanned position of worn track on the NiCoCrAlY coating with the B<sub>4</sub>C mass fraction of 15%. The Ni, Cr and Al contents



**Fig. 8** Line scan analysis of worn track on NiCoCrAlY coating: (a) Line scanned position; (b) Contents of Ni, Co, Cr and Al; (c) Contents of Ti, Si and O



**Fig. 9** Line scan analysis of worn track on NiCoCrAlY coating with B<sub>4</sub>C mass fraction of 5%: (a) Line scanned position; (b) Contents of Ni, Co, Cr and Al; (c) Contents of Ti, O and Si

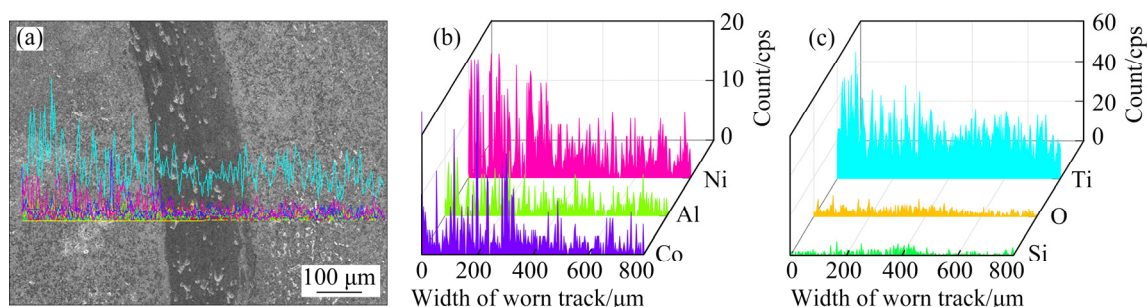


**Fig. 10** Line scan analysis of worn track on NiCoCrAlY coating with B<sub>4</sub>C mass fraction of 10%: (a) Line scanned position; (b) Contents of Ni, Co and Al; (c) Contents of Ti, O and Si

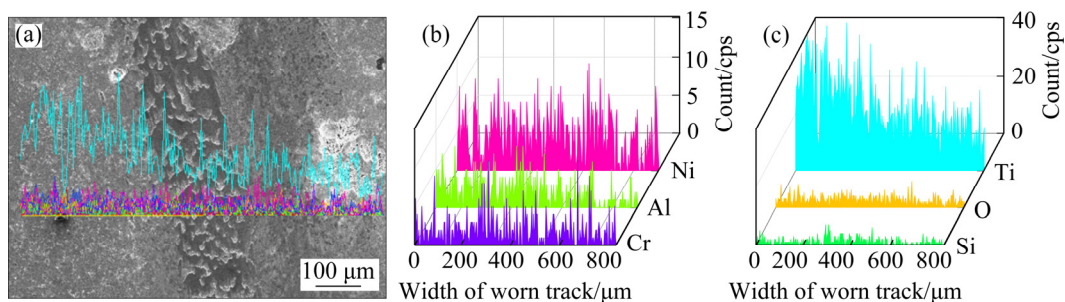


**Fig. 11** Line scan analysis of worn track on NiCoCrAlY coating with B<sub>4</sub>C mass fraction of 15%: (a) Line scanned position; (b) Contents of Ni, Cr and Al; (c) Contents of Ti, O and Si

on the worn track changed little than the unworn coating, as shown in Fig.11 (b). The Ti content on the worn track decreased slightly than the unworn coating, while the O content did not changed, indicating that the degree of oxidation wear was further reduced. The Si content on the worn track increased than the unworn coating, indicating that the adhesive wear occurred in the friction process, as shown in Fig. 11(c).

From the above analysis, it can be seen that the Ti content on the worn tracks of NiCoCrAlY–B<sub>4</sub>C coatings was lower than the NiCoCrAlY coating, which was because the TiC and TiB occupied the original Ti position of substrate and reduced the content of  $\alpha$ -Ti. Meanwhile, the O content on the worn track decreased with the increase of B<sub>4</sub>C mass fraction, which indicated that the degree of oxidation wear decreased to a certain extent.

### 3.3.4 Wear mechanism

Figure 12(a) shows the wear mechanism on the early friction process of NiCoCrAlY–B<sub>4</sub>C coatings. The oxide layer produced by the tribochemistry reaction at high temperature was formed on the coating surface [27], and the exfoliated oxides were adhered to the contact point on the coating due to its friction heat, indicating that the adhesive wear occurred on the pink zones. The TiB, TiC and other hard phases gathered on the worn track in the early friction process, and the cutting effect of tribo-pair on the coating was hindered to improve the wear resistance of coating. Under the action of reciprocating normal force, the fatigue cracks were formed at the boundaries of hard phases and marked red zones. In the subsequent normal friction process, part of the hard phases fell off from the coating surface and formed fatigue pittings, which was related to the number of hard phases, as shown in Fig. 12(b).

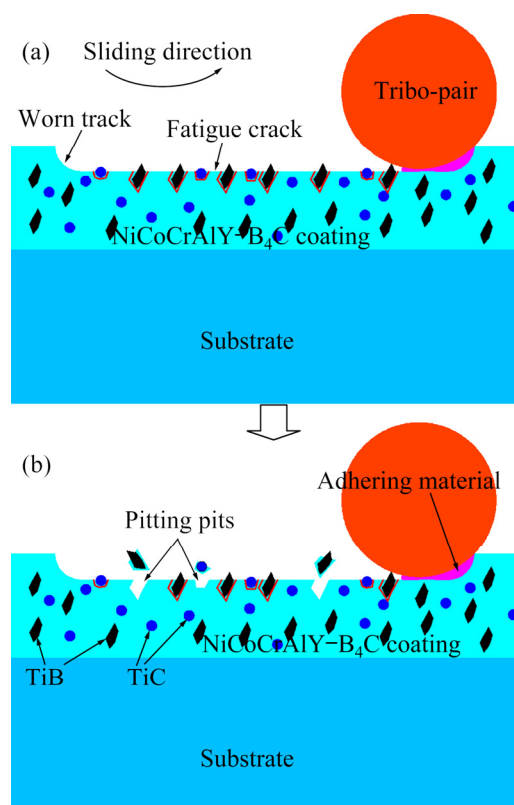


**Fig. 12** Sketches of wear mechanism of NiCoCrAlY–B<sub>4</sub>C coatings in early (a) and normal (b) friction processes

## 4 Conclusions

(1) The NiCoCrAlY–B<sub>4</sub>C coatings are mainly composed of NiTi, NiTi<sub>2</sub>, CoO, TiB, TiC, TiB<sub>2</sub>, AlB<sub>2</sub> and  $\alpha$ -Ti phases, and the (Ni,CO)<sub>2</sub>Ti<sub>4</sub>O and rutile-TiO<sub>2</sub> new phases are formed on the NiCoCrAlY–B<sub>4</sub>C coatings after the high temperature wear test.

(2) The addition of B<sub>4</sub>C reduces the precipitation of  $\alpha$ -Ti and the dendrite disappears on the NiCoCrAlY–B<sub>4</sub>C coating, the hardnesses of NiCoCrAlY coatings with the B<sub>4</sub>C mass fractions of

5%, 10% and 15% are HV 1002, HV 1054, and HV 1213, respectively, higher than HV 893 of NiCoCrAlY coating.

(3) The B<sub>4</sub>C addition plays a certain role in the reduction friction, and the average COFs of NiCoCrAlY coatings with the B<sub>4</sub>C mass fractions of 5%, 10% and 15% are 0.31, 0.29, and 0.26, respectively, which decrease with the increase of B<sub>4</sub>C mass fraction.

(4) The wear rates of NiCoCrAlY coatings with the B<sub>4</sub>C mass fractions of 5%, 10% and 15% are  $9.16 \times 10^{-6}$ ,  $8.46 \times 10^{-6}$ , and  $5.45 \times 10^{-6}$  mm<sup>3</sup>/(N·m), respectively, which decrease by 61.63%, 64.58%, and 77.17% compared with  $23.89 \times 10^{-6}$  mm<sup>3</sup>/(N·m) of NiCoCrAlY coating, respectively.

(5) The TiC and TiB phases are in-situ synthesized by the reactions of B<sub>4</sub>C and Ti on the NiCoCrAlY–B<sub>4</sub>C coatings, which reduce the adhesive wear and oxidation wear, and the fatigue wear increases with the mass fraction of B<sub>4</sub>C.

## References

- [1] YANG Xin, WANG Wan-lin, MA Wen-jun, WANG Yan, YANG Jun-gang, LIU Shi-feng, TANG Hui-ping. Corrosion and wear properties of micro-arc oxidation treated Ti6Al4V alloy prepared by selective electron beam melting [J]. Transactions of Nonferrous Metals Society of China, 2020, 30(8): 2132–2142.
- [2] LI G J, LI J, LUO X. Effects of post-heat treatment on microstructure and properties of laser clad composite coatings on titanium alloy substrate [J]. Optics and Laser Technology, 2015, 65: 66–75.
- [3] LI Jun, WANG Hui-ping, LI Mang-ping, YU Zhi-shui. Effect of yttrium on microstructure and mechanical properties of laser clad coatings reinforced by in situ synthesized TiB and TiC [J]. Journal of Rare Earths, 2011, 29 (5): 477–483.
- [4] JIN Lei, LI Pei-zhong, ZHOU Hai-bin, ZHANG Wei, ZHOU Guo-dong, WANG Chun. Improving thermal insulation of TC4 using YSZ-based coating and SiO<sub>2</sub> aerogel [J]. Progress in Natural Science: Materials International, 2015, 25(2): 141–146.
- [5] PEREIRA J, ZAMBRANO J, LICAUSI M, TOBAR M, AMIGÓ V. Tribology and high temperature friction wear behavior of MCrAlY laser cladding coatings on stainless steel [J]. Wear, 2015, 330: 280–287.
- [6] PEREIRA FALCON J C, ECHEVERRIA A, AFONSO C R M, ZAMBRANO CARRULLO J C, AMIGO BORRAS V. Microstructure assessment at high temperature in NiCoCrAlY overlay coating obtained by laser metal deposition [J]. Journal of Materials Research and Technology, 2019, 8(2): 1761–1772.
- [7] HU Miao, CHENG Tang-jian, CHEN Xin-gui, YE Nan, ZHAO Xin-yue, XU Miao-miao. Microstructure and properties of WC–12Co composite coatings prepared by laser cladding [J]. Transactions of Nonferrous Metals Society of China, 2020, 30(4): 1017–1030.
- [8] SALIMIJAZI H R, COYLE T W, MOSTAGHIMI J, LEBLANC L. Microstructure of vacuum plasma-sprayed boron carbide [J]. Journal of Thermal Spray Technology, 2005, 14: 362–368.
- [9] GREUNER H, BALDEN M, BOESWIRTH B, BOLT H, GADOW R, GRIGULL P, HOFMANN G, HUBER T, KASPAREK W, KUMRIC H, LINDIG S, MATERN G, MAYER M, NEU R, RENNER H, ROTH J, RIEGERT–ESCRIBANO M, SIMON–WEIDNER J, WACKER R. Evaluation of vacuum plasma-sprayed boron carbide protection for the stainless steel first wall of WENDELSTEIN 7–X [J]. Journal of Nuclear Materials, 2004, 329–333: 849–854.
- [10] CAO Si-long, REN Shu-fang, ZHOU Jian-song, YU You-jun, WANG Ling-qian, GUO Chun, XIN Ben-bin. Influence of composition and microstructure on the tribological property of SPS sintered MCrAlY alloys at elevated temperatures [J]. Journal of Alloys and Compounds, 2018, 740: 790–800.
- [11] PUSHPANATHAN D P, ALAGUMURTHI N, DEVANEYAN S P. On the microstructure and tribological properties of pulse electrodeposited Ni–B<sub>4</sub>C–TiC nano composite coating on AZ80 magnesium alloy [J]. Surfaces and Interfaces, 2020, 19: 100465.
- [12] MENG Q W, GENG L, ZHANG B Y. Laser cladding of Ni-base composite coatings onto Ti–6Al–4V substrates with pre-placed B<sub>4</sub>C+NiCrBSi powders [J]. Surface and Coatings Technology, 2006, 200(16–17): 4923–492.
- [13] HORIUUCHI Y, INAMURA T, KIM H Y, WAKASHIMA K, MIYAZAKI S, HOSODA H. Effect of boron concentration on martensitic transformation temperatures, stress for inducing martensite and slip stress of Ti24mol%–Nb3mol%Al superelastic alloy [J]. Materials Transactions, 2007, 48(3): 407–413.
- [14] SUN Jun-long, LIU Chang-xia, WANG Ru-gui. Low pressure hot pressing of B<sub>4</sub>C matrix ceramic composites improved by Al<sub>2</sub>O<sub>3</sub> and TiC additives [J]. Materials Science and Engineering A, 2009, 519 (1): 27–31.
- [15] LI J, LUO X, LI G J. Effect of Y<sub>2</sub>O<sub>3</sub> on the sliding wear resistance of TiB/TiC-reinforced composite coatings fabricated by laser cladding [J]. Wear, 2014, 310 (1): 72–82.
- [16] SUN R L, MAO J F, YANG D Z. Microscopic morphology and distribution of TiC phase in laser clad NiCrBSiC–TiC layer on titanium alloy substrate [J]. Surface and Coatings Technology, 2002, 155 (2): 203–207.
- [17] ZHAO Yu, YU Tian-biao, GUAN Chuang, SUN Jia-yu, TAN Xue-fei. Microstructure and friction coefficient of ceramic (TiC, TiN and B<sub>4</sub>C) reinforced Ni-based coating by laser cladding [J]. Ceramics International, 2019, 45(16): 20824–20836.
- [18] CAI Chao, RADOSLAW C, ZHANG Jin-liang, YAN Qian, WEN Shi-feng, SONG Bo, SHI Yu-sheng. In-situ preparation and formation of TiB/Ti–6Al–4V nanocomposite via laser additive manufacturing: Microstructure evolution and tribological behavior [J]. Powder Technology, 2019, 342: 73–84.
- [19] ZHAO Yu, YU Tian-biao, CHEN Liao-yuan, CHEN Ying, GUAN Chuang, SUN Jia-yu. Microstructure and wear

- resistance behavior of Ti–C–B<sub>4</sub>C-reinforced composite coating [J]. *Ceramics International*, 2020, 46(16): 25136–25148.
- [20] WANG Hong-yu, ZUO Dun-wen, LI Xiang-feng, CHEN Kang-min, HUANG Ming-min. Effects of CeO<sub>2</sub> nanoparticles on microstructure and properties of laser cladded NiCoCrAlY coatings [J]. *Journal of Rare Earths*, 2010, 28(2): 246–250.
- [21] HUSSAIN M, MANDAL V, SINGH P K, KUMAR P, KUMAR V, DAS A K. Experimental study of microstructure, mechanical and tribological properties of cBN particulates SS316 alloy based MMCs fabricated by DMLS technique [J]. *Journal of Mechanical Science and Technology*, 2017, 31: 2729–2737.
- [22] HUANG L J, GENG L, PENG H X. Microstructurally inhomogeneous composites: Is a homogeneous reinforcement distribution optimal? [J]. *Progress in Materials Science*, 2015, 71: 93–168.
- [23] WANG Si-yang, ZHOU Hong, ZHANG Peng, CHEN Huan-xi, LI Hui, MA Si-yuan, CHANG Geng, ZHI Ben-feng, ZHAO Shi-zhe. Effect of different hardness units on fatigue wear resistance of low hardenability steel [J]. *Optics and Laser Technology*, 2020, 130: 106325.
- [24] GUO Chun, CHEN Jian-min, YAO Run-gang, ZHOU Jian-song. Microstructure and high temperature wear resistance of laser cladding NiCoCrAlY/ZrB<sub>2</sub> coating [J]. *Rare Metal Materials and Engineering*, 2013, 42(8): 1547–1551.
- [25] CHUPRINA V G, SHALYA I M. Reactions of TiNi with oxygen [J]. *Powder Metallurgy and Metal Ceramics*, 2002, 41: 85–89.
- [26] QIN Yu-mei, WANG Zi-ning, JIANG Juan-tao, XING Ling-bo, WU Kai. One-step fabrication of TiO<sub>2</sub>/Ti foil annular photoreactor for photocatalytic degradation of formaldehyde [J]. *Chemical Engineering Journal*, 2020, 394: 124917.
- [27] WANG Hong-yu, ZUO Dun-wen, WANG Ming-di, SUN Gui-fang, MIAO Hong, SUN Yu-li. High temperature frictional wear behaviors of nano-particle reinforced NiCoCrAlY cladded coatings [J]. *Transactions of Nonferrous Metals Society of China*, 2011, 21(6): 1322–1328.

## Ti6Al4V 合金表面激光熔覆 NiCoCrAlY–B<sub>4</sub>C 复合涂层的结构特征及高温摩擦学性能

王文昌<sup>1</sup>, 李嘉兴<sup>2</sup>, 葛源<sup>3</sup>, 孔德军<sup>2</sup>

1. 常州大学 石油化工学院, 常州 213164;
2. 常州大学 机械工程学院, 常州 213164;
3. 熔创金属表面技术(常州)有限公司, 常州 213164

**摘要:** 为提高 Ti6Al4V 合金的硬度和摩擦学性能, 采用激光熔覆技术在其表面制备 NiCoCrAlY–B<sub>4</sub>C 复合涂层 (B<sub>4</sub>C 的质量分数分别为 5%、10%和 15%)。利用扫描电子显微镜(SEM)、能谱仪(EDS)和 X 射线衍射仪(XRD)对所制备涂层的形貌、化学成分和物相进行分析, 并采用球–盘磨损试验机研究 B<sub>4</sub>C 质量分数对 NiCoCrAlY–B<sub>4</sub>C 涂层在 600 °C 时摩擦因数和磨损率的影响。结果表明, 不同 B<sub>4</sub>C 质量分数的 NiCoCrAlY–B<sub>4</sub>C 涂层主要由 NiTi、NiTi<sub>2</sub>、 $\alpha$ -Ti、CoO、AlB<sub>2</sub>、TiC、TiB 和 TiB<sub>2</sub> 物相组成。NiCoCrAlY–B<sub>4</sub>C 涂层的平均摩擦因数和磨损率随着 B<sub>4</sub>C 质量分数的增加而有所降低, 主要归因于 B<sub>4</sub>C 的添加提高了涂层硬度。随着 B<sub>4</sub>C 质量分数的增加, NiCoCrAlY–B<sub>4</sub>C 涂层的磨损机制由粘着磨损、氧化磨损转变为疲劳磨损。

**关键词:** Ti6Al4V 合金; 激光熔覆; NiCoCrAlY 涂层; B<sub>4</sub>C; 摩擦行为; 磨损

(Edited by Xiang-qun LI)